



**SPE 118993**

## **A Multiscale Mixed Finite-Element Solver for Three-Phase Black-Oil Flow**

S. Krogstad, K.-A. Lie, H. Møll Nilsen, J. R. Natvig, B. Skaflestad, and J. E. Aarnes, SINTEF

Copyright 2009, Society of Petroleum Engineers

This paper was prepared for presentation at the 2009 SPE Reservoir Simulation Symposium held in The Woodlands, Texas, USA., 2-4 February 2009.

This paper was selected for presentation by an SPE program committee following review of information contained in an abstract submitted by the author(s). Contents of the paper have not been reviewed by the Society of Petroleum Engineers and are subject to correction by the author(s). The material does not necessarily reflect any position of the Society of Petroleum Engineers, its officers, or members. Electronic reproduction, distribution, or storage of any part of this paper without the written consent of the Society of Petroleum Engineers is prohibited. Permission to reproduce in print is restricted to an abstract of not more than 300 words; illustrations may not be copied. The abstract must contain conspicuous acknowledgment of SPE copyright.

### **Abstract**

Previous research has shown that multiscale methods are robust and capable of providing more accurate solutions than traditional upscaling methods. Multiscale methods solve the pressure equation on a coarse grid, but capture the effects from fine-scale heterogeneities through basis functions computed numerically from local single-phase problems on the underlying geocellular grid. Published results have so far been limited to simple Cartesian grids and/or incompressible flow. Here, we present a multiscale mixed finite-element method for three-phase black-oil flow on geomodels with industry-standard complexity. In particular, we discuss which effects can be incorporated in the multiscale basis functions and which effects should be modeled only on the coarsened simulation grid. Moreover, we describe how to handle degenerate hexahedral cells and non-matching interfaces that occur across faults. Finally, we present results of flow simulations on models of industry-standard complexity and demonstrate how multiscale methods can be used to simulate three-phase black-oil flow directly on high-resolution geomodels. The multiscale methods presented herein enable varying resolution and provide a systematic procedure for coarsening or refining the simulation model.

### **Introduction**

For the oil industry to succeed in increasing oil recovery there is a growing trend for model-based decisions. New and exciting developments are seen in a variety of areas such as real-time reservoir management, uncertainty quantification, integrated operations, closed-loop management, and production optimization. Common to all these fields of endeavor is the requirement for fast flow simulation in which the simulation model is tightly coupled to the geology and dynamic data sources.

However, there is a significant, and increasing, gap between the level of detail seen in geological models and the capabilities of contemporary reservoir simulators. Mature fields have a large amount of geological and geophysical data that can be used to create static models, and sizes of high-resolution geological models range from a few million and up to a billion cells. Contemporary reservoir simulators typically operate on model sizes from tens of thousands to a few million cells. Similarly, mature fields usually have a lot of dynamic data (pressure tests, production data, 4-D seismics, etc) that could be used to calibrate and history match the high-resolution geological models. Unfortunately, instead of focusing on understanding the physical characteristics of reservoirs and the economic consequences of different developments, a lot of valuable human resources is diverted to upscaling (and downscaling) and its negative consequences for the representation of heterogeneities and fluid flow. Upscaling is a costly process which additionally wastes much of the information inherent in high-resolution geological models since local flow structures are only preserved in an average sense on the upscaled grid. Enabling the oil industry to make a step-change in its work processes therefore calls for a radical speedup of flow simulation and for simulators that are equipped to utilize both static data and the vast amount of dynamic data that becomes available. As an example, it would be highly attractive if reservoir simulation could be performed at seismic resolution in order to use 4-D seismics to history-match simulation models.

There are several technological developments that can contribute to a radical speedup of flow simulation: advances in hardware, parallel algorithms, improved (non)linear solvers, and alternative formulations (streamlines, operator splitting), to name a few. Another important contribution may come from multiscale methods, as will be discussed herein. Generally speaking, multiscale methods are numerical methods and strategies that aim to describe physical phenomena on coarse grids while accounting for the influence of fine-scale structures in the porous media. However, unlike traditional upscaling techniques, multiscale methods often provide a mechanism to recover an approximate fine-scale solutions.

Multiscale modeling of flow and transport in porous media has become a hot research topic in recent years. A quite comprehensive overview of current developments is found in a recent issue of the *Computational Geosciences* journal (Juanes and Tchelepi 2008). Common for all these methods is that they seek efficient solutions of elliptic (or parabolic) equations with rough coefficients in the absence of scale separation, which is often assumed in many other multiscale methods. In the race for making a

multiscale method that is capable of solving problems with industry-standard complexity both with regard flow physics and grid types, there are currently two main contenders that both stem from the seminal paper of Hou and Wu (1997).

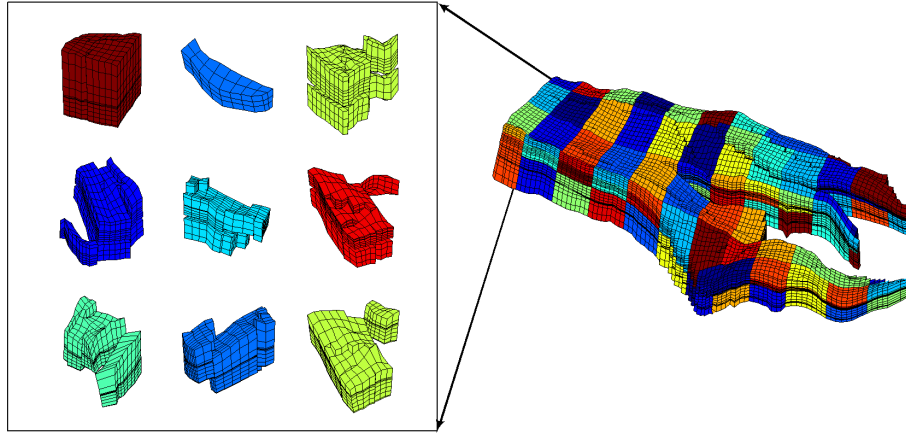
The multiscale finite-volume (MsFV) method (Jenny et al. 2003) is based on a control-volume approach and formulated using dual grids, on which multiscale basis functions for pressure are developed. Conservative flux approximations are obtained by adding an extra reconstruction step on the primal grids. Early versions of the method were formulated for incompressible two-phase flow on Cartesian grids, and later development has mainly focused on inclusion of more complex physics, including compressibility (Lunati and Jenny 2006), gravity (Lunati and Jenny 2008), and black-oil models (Lee et al. 2008). Recent versions of the MsFV method (Hajibeygi et al. 2008) are strongly reminiscent of a multigrid method (see, for instance, Zhou and Tchelepi 2008) and seem to aim at driving the residuals of the fine-scale discretization towards zero by introducing advanced fine-scale reconstructions and (costly) iterations.

The second contender, the multiscale mixed finite-element (MsMFE) method (Chen and Hou 2003), is based on a mixed finite-element formulation and avoids the introduction of a dual grid. The method is therefore more flexible with respect to complex grids, and recent developments include extensions to nonuniform coarse grids (Aarnes et al. 2006) and to corner-point and other unstructured grids (Aarnes et al. 2008). In the most recent version of the MsMFE method (Aarnes et al. 2008), the underlying mixed discretization has been replaced by a mimetic method that is applicable to general polyhedral grids and can be classified as a multipoint flux-approximation scheme. The current paper presents two new contributions for the MsMFE methodology. First of all, we present the first extension to compressible black-oil models. Second, in order to do so, we reformulate the pressure approximation space to include fine-grid variations. To prepare for the technical discussion that will follow in the rest of the paper, we will now give a quick (visual) overview of the MsMFE method. The method is formulated using two (hierarchically nested) grids: a fine-scale grid on which the rock and rock-fluid properties are given and a coarse simulation grid to which we associate the degrees-of-freedom used to solve the global flow problem. Briefly explained, a flow simulation using the MsMFE method is performed according to the following algorithm:

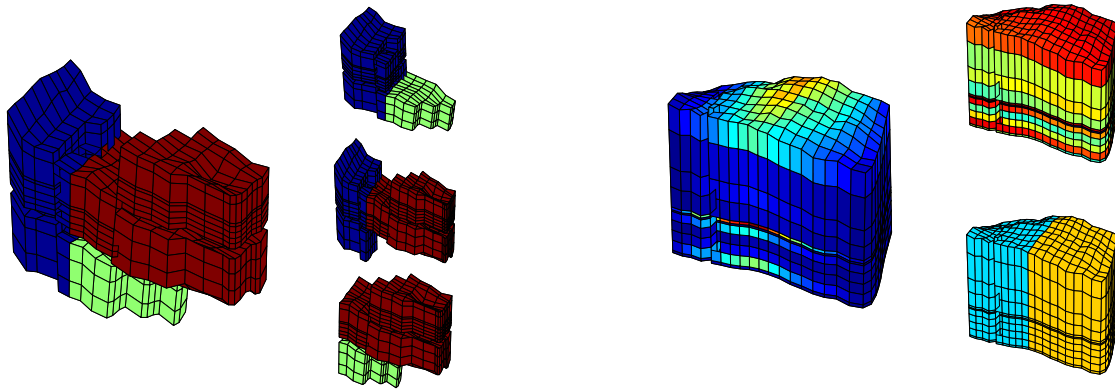
1. First we introduce a coarse grid for which each block consists of a connected collection of cells from the underlying fine grid, as seen in **Fig. 1a**. For corner-point grids the simplest and yet most effective approach is to partition the input grid in index-space, using e.g., a uniform partitioning in which each coarse block is assigned an equal number of cells in index space. This may give highly irregular block geometries, as seen in Fig. 1a, but preserves geological structures, simplifies the coupling in the resulting linear system, and most importantly, enables automatic coarsening of grids. We refer the reader to Aarnes et al. (2008) for a more thorough discussion and some simple guidelines on how to generate good coarse grids.
2. Next, we detect all pairs of adjacent gridblocks, as illustrated for a small subdomain of the field in Fig. 1b.
3. For each pair of adjacent gridblocks, we solve a local flow problem numerically to determine basis functions, as shown in Fig. 1c, that will later be used as building blocks for constructing the global solution; see Fig. 1d. The exact formulation and discretization of the local flow problems is discussed in full detail in the next section.
4. For each time-step in the simulation we:
  - (a) Check if any basis functions require recomputing; more details about this later.
  - (b) Assemble the coarse-grid system using the variational form from the corresponding mixed finite-element formulation, which amounts to integrating multiscale basis functions and computing their interaction. In a practical implementation, this is done by matrix vector multiplication, as will be explained in more detail in the next section.
  - (c) Recover pressures and velocities/fluxes on the underlying fine grid. This is achieved directly using the subgrid resolution in the multiscale basis function.
  - (d) Solve the fluid-transport equations using the fine-scale pressures and fluxes, which are assumed to be constant in time.

For increased stability, one may iterate on solving the pressure and transport equations before advancing to the next time step and thereby obtain a fully implicit method (Jenny et al. 2006; Lu et al. 2007).

From a computational point-of-view, the resulting algorithm has several appealing features. First of all, multiscale methods are very robust with respect to the coarsening factor (Kippe et al. 2008). Second, the method can be built on top of any pre-existing (conservative) pressure solver on the fine grid. Third, the MsMFE method provides a mass-conservative velocity on the fine grid without downscaling (i.e., without having to solve a local problem within each coarse block to reconstruct fluxes as e.g., in the multiscale finite-volume method (Jenny et al. 2006)). When used as an approximate fine-grid solver, the MsMFE method has a natural parallelism that can be exploited on multicore and parallel computers. Finally, multiscale methods are naturally suited for adaptive strategies in which the subresolution in velocity is used only when required. Herein, we will always assume the classical multiscale modeling approach in which the MsMFE method is used on a coarse simulation grid defined over a fine input grid; however, as suggested by Natvig et al. (2009), the MsMFE method could equally well be used to incorporate high-impact details that are not represented in the input grid.

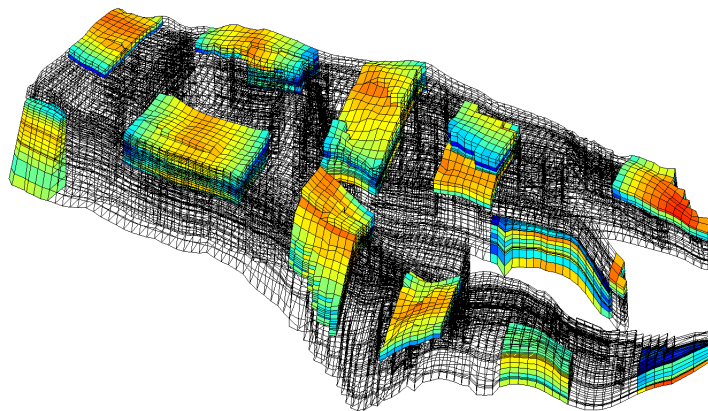


(a) Introduce a coarse grid by partitioning the input grid in index space, as seen in the right plot. The left plot shows a selection of nine coarse gridblocks.



(b) Detect all pairs of adjacent blocks, as illustrated for a small sub-domain consisting of three adjacent coarse gridblocks. Basis functions are to be computed for each pair of gridblocks that share a common interface.

(c) Compute a basis function for each pair of coarse gridblocks. The left plot shows the velocity magnitude for a basis function modeling flow between the two adjacent gridblocks depicted in the bottom right plot. In the top right plot we show the logarithm of the corresponding permeability field.



(d) A selection of velocity basis functions shown in the global reservoir model. All basis functions model fine-grid flow patterns between two adjacent gridblocks. The MsMFE velocity solution is expressed as a linear superposition of all velocity basis functions.

**Fig. 1—A visual illustration of key steps in the multiscale mixed finite-element simulation algorithm using a corner-point grid with industry-standard complexity.**

## Model and Fine-Scale Discretization

We consider compressible three-phase flow in porous media for which capillarity is neglected. For simplicity, we only consider immiscible flow without gravity; extension to miscible flow and inclusion of gravity are straightforward. The governing equations are the standard mass-conservation equations of the three phases inside a computational domain  $\Omega$  with boundary  $\partial\Omega$ ,

$$\frac{\partial(\phi b_\ell s_\ell)}{\partial t} + \nabla \cdot (b_\ell \vec{u}_\ell) = q_\ell, \quad \vec{u}_\ell = -\lambda_\ell \mathbf{K} \nabla p \text{ in } \Omega, \quad (1)$$

where  $\ell = o, w, g$  denotes the three phases;  $\phi$  is the porosity;  $b_\ell$  is the inverse of the phase formation volume factor (ratio of density at reservoir condition to density at surface conditions);  $s_\ell$  is the phase saturation;  $\vec{u}_\ell$  is the phase volumetric flux (at reservoir conditions);  $q_\ell$  is the source term;  $\mathbf{K}$  is the absolute permeability;  $\lambda_\ell = k_{r\ell}/\mu_\ell$  is the phase mobility, where  $k_{r\ell}$  is the relative permeability, and  $\mu_\ell$  is the phase viscosity.

In the following we assume that the system Eq. 1 is solved using an operator splitting method in which the flow (pressure and total velocity) and transport problems are solved separately, using an IMPES-like method or the sequential fully-implicit method (Tchelepi et al. 2007). To derive the pressure equation, we multiply the first equation in Eq. 1 by  $b_\ell^{-1}$ , use the chain rule and sum over all three phases to eliminate saturation. Then insert the expression for the Darcy velocities, and eliminate  $\nabla p$  to give

$$c_t \frac{\partial p}{\partial t} + \nabla \cdot \vec{u} - \zeta \vec{u} \cdot (\lambda \mathbf{K})^{-1} \vec{u} = q. \quad (2)$$

Here  $\vec{u} = -\lambda \mathbf{K} \nabla p$  is the total Darcy velocity, where  $\lambda = \sum \lambda_\ell$  is the total mobility;  $\zeta$  is shorthand for  $\sum c_\ell f_\ell$ , where  $f_\ell = \lambda^{-1} \lambda_\ell$  is the fractional flow;  $q = \sum q_\ell / b_\ell$  is the total source; and  $c_\ell$  and  $c_t$  are the phase and total compressibilities given by

$$c_\ell = \frac{d \ln b_\ell}{dp}, \quad c_t = \frac{d\phi}{dp} + \phi \sum_\ell c_\ell s_\ell. \quad (3)$$

For simplicity, we assume that Eq. 2 is only equipped with Neumann boundary conditions  $\vec{u} \cdot \vec{n} = b_N$ , where  $\vec{n}$  is the outward normal of  $\partial\Omega$ . A key point in our method is to represent wells as boundary conditions. Hence, a well  $w$  with boundary  $\gamma_w$  is conceptually represented as a *hole* in  $\Omega$  with  $\gamma_w \subset \partial\Omega$  and Eq. 2 can therefore be considered as free of source. We consider wells that are either pressure constrained ( $p = p^w$  on  $\gamma_w$ ) or rate constrained ( $\int_{\gamma_w} \vec{u} \cdot \vec{n} = -q_w$  on  $\gamma_w$ ). See Skaflestad and Krogstad (2008) for more details on the representation of wells.

Pressure equation Eq. 2 remains valid for miscible flows if the phase compressibilities are defined to also include compressibility of the solution gas-oil ratios etc. Moreover, if gravity is included, the third term on the left-hand side takes the form

$$(\zeta \vec{u} + \beta \vec{g}) \cdot ((\lambda \mathbf{K})^{-1} \vec{u} + \omega \vec{g}).$$

In either case, the derivations presented in the next subsections can be repeated verbatim, but with more complex algebraic expressions.

**Discretization and Hybrid System.** To provide a background for the multiscale methods to be introduced below, we start by discussing the direct fine-grid discretization of Eq. 2 in some detail. We start by assuming that the computational domain  $\Omega$  is represented by a grid consisting of a set  $\{E_i\}$  of  $N$  polyhedral cells in which each cell  $E$  can have a varying number of  $n_E$  planar faces. For a corner-point grid, each non-degenerate cell has  $n_E = 6$  faces, whereas  $n_E < 6$  for degenerate cells (eroded cells, pinch-out cells, etc) that are not neighbor to a fault. At faults, we subdivide all faces into a set of new polygonal faces so that a cell shares a single polygonal face with each of its intersecting neighbors. In other words, if a cell has three neighbors across a fault, the corresponding face is replaced by three new polygonal faces. All faces are assumed to be planar with the face area computed from a triangulation that is unique for each face. Similarly, the normal vector is computed as the area-weighted average of the normal vectors of the subtriangles.

Now, let  $\mathbf{u}_E$  be the vector of outward fluxes of the faces of  $E$ ,  $p_E$  the pressure at the cell center, and  $\boldsymbol{\pi}_E$  the pressures at the cell faces. Most discretization methods used for reservoir simulation relate these quantities through a *transmissibility* matrix  $\mathbf{T}_E$  such that

$$\mathbf{u}_E = \lambda(s_E) \mathbf{T}_E (p_E - \boldsymbol{\pi}_E). \quad (4)$$

Examples include the two-point flux-approximation (TPFA) method (see e.g., Aziz and Settari 1979), the lowest-order mixed finite-element (MFE) methods (see e.g., Brezzi and Fortin 1991), and recent mimetic finite-difference (MFD) methods by Brezzi et al. (2005). While MFE and MFD methods in general lead to full  $\mathbf{T}_E$ -matrices, the TPFA discretization results in a diagonal  $\mathbf{T}_E$ , but is nonconvergent for general grids. We refer the reader to the cited references for details on the computation of  $\mathbf{T}_E$  for each method. To efficiently handle polyhedral cells, we will in the following use MFDM as our default discretization method. In our experience, this method is very flexible and not very sensitive to the geometry of the cell or the number of faces and corner-points. On Cartesian grids, we will use the simpler TPFA scheme.

To derive a discretization of Eq. 2, we let  $\mathbf{u}$  denote the face outward fluxes ordered cell-wise (thus, fluxes on interior faces appear twice with opposite signs),  $s$  the cell-wise saturations,  $\mathbf{p}$  the cell pressures, and  $\boldsymbol{\pi}$  the face pressures. These are all assumed to be known from the previous time step  $t^n$ . The accumulation term  $c_t \frac{\partial p}{\partial t}$  in Eq. 2 is then approximated by a backward time-difference and all coefficients except  $s$  are evaluated at the new time step  $t^{n+1}$ . This gives a system of nonlinear equations, which we linearize and solve iteratively. That is, we set  $\mathbf{u}_0 = \mathbf{u}^n$ ,  $\mathbf{p}_0 = \mathbf{p}^n$ , and  $\boldsymbol{\pi}_0 = \boldsymbol{\pi}^n$  and iteratively solve the linearized, hybrid system

$$\begin{bmatrix} \mathbf{B} & \mathbf{C} & \mathbf{D} \\ \mathbf{C}^\top - \mathbf{V}^\top(\mathbf{u}_\nu) & \mathbf{P} & \mathbf{0} \\ \mathbf{D}^\top & \mathbf{0} & \mathbf{0} \end{bmatrix} \begin{bmatrix} \mathbf{u}_{\nu+1} \\ -\mathbf{p}_{\nu+1} \\ \boldsymbol{\pi}_{\nu+1} \end{bmatrix} = \begin{bmatrix} \mathbf{0} \\ \mathbf{P}\mathbf{p}^n \\ \mathbf{b}_N \end{bmatrix} \quad (5)$$

until  $\|\mathbf{p}_{\nu+1} - \mathbf{p}_\nu\|$  and  $\|\mathbf{u}_{\nu+1} - \mathbf{u}_\nu\|$  are sufficiently small. The matrix  $\mathbf{P}$  is diagonal with entry  $(c_t|E|/\Delta t)$  for cell  $E$ . The matrices  $\mathbf{B}$  and  $\mathbf{C}$  are block diagonal and for which the gridblocks corresponding to cell  $E$  are  $(\lambda(s_E)\mathbf{T}_E)^{-1}$  and an  $n_E \times 1$  vector with all entries equal one, respectively. If  $\mathbf{D}_\zeta$  and  $\mathbf{D}_u$  denote diagonal matrices with  $\zeta$  and  $\mathbf{u}$  on the diagonal, then the block matrix  $\mathbf{V}(\mathbf{u})$  is given by  $\mathbf{B}\mathbf{D}_u\mathbf{C}\mathbf{D}_\zeta$ . Finally, each column of  $\mathbf{D}$  corresponds to a unique face and has one or two unit entries (for boundary and interior faces, respectively) corresponding to the index/indices of the face in the cell-wise ordering. On the right-hand side,  $\mathbf{b}_N$  corresponds to flux (Neumann) boundary conditions. To incorporate Dirichlet boundary conditions (e.g., pressure-constrained wells) in Eq. 5, one can split  $\boldsymbol{\pi}$  and  $\mathbf{D}$  in two parts, where the first part corresponds to interior and Neumann faces and the second corresponds to Dirichlet faces that can be eliminated from the linear system; see Skaflestad and Krogstad (2008) for more details.

When the iteration Eq. 5 has converged, we set  $\mathbf{u}^{n+1} = \mathbf{u}_{\nu+1}$ ,  $\mathbf{p}^{n+1} = \mathbf{p}_{\nu+1}$ , and  $\boldsymbol{\pi}^{n+1} = \boldsymbol{\pi}_{\nu+1}$  and use the updated pressure and total velocity to advance the saturation to time  $t^{n+1}$ . Because the flow and transport equations are nonlinearly coupled, we may need to solve the pressure equation Eq. 2 again using the new saturation  $s^{n+1}$  to evaluate saturation-dependent parameters and reiterate the complete time step to ensure that pressure and total velocity are consistent with the saturation.

**Wells as Boundary Conditions.** Wells are modeled using well indices (Peaceman 1983)  $q_w = -\lambda(s_E)WI(p_E - p_w)$ , where  $q_w$  is the well rate,  $\lambda$  is the total mobility,  $WI$  is the well index,  $p_w$  is the well pressure, and  $p_E$  is the pressure in the perforated cell  $E$ . Assume a system with  $N_w$  wells, and that well  $w_k$  perforates  $n_k$  cells  $E_{k_i}$ ,  $i = 1, \dots, n_k$ , each with a well index  $WI_i^k$ . The set of equations for all wells is then given, for  $k = 1, \dots, N_w$ ,

$$q_{w_k}^{\text{tot}} = \sum_{i=1}^{n_k} q_i^k, \quad -q_i^k = \lambda(s_{k_i})WI_i^k(p_{E_{k_i}} - p_{w_k}), \quad i = 1, \dots, n_k. \quad (6)$$

We now assume noflow boundary conditions everywhere except at wells and no additional sources. Then Eq. 6 can be coupled with the linearized system Eq. 5 to form an extended linear system (where we for simplicity drop the iteration parameter  $\nu$ )

$$\begin{bmatrix} \mathbf{B} & \mathbf{0} & \mathbf{C} & \mathbf{D} & \mathbf{0} \\ \mathbf{0} & \mathbf{B}_w & \mathbf{C}_w & \mathbf{0} & \mathbf{D}_w \\ \mathbf{C}^\top - \mathbf{V}^\top & \mathbf{C}_w^\top - \mathbf{V}_w^\top & \mathbf{P} & \mathbf{0} & \mathbf{0} \\ \mathbf{D}^\top & \mathbf{0} & \mathbf{0} & \mathbf{0} & \mathbf{0} \\ \mathbf{0} & \mathbf{D}_w^\top & \mathbf{0} & \mathbf{0} & \mathbf{0} \end{bmatrix} \begin{bmatrix} \mathbf{u} \\ -\mathbf{q}_w \\ -\mathbf{p} \\ \boldsymbol{\pi} \\ \mathbf{p}_w \end{bmatrix} = \begin{bmatrix} \mathbf{0} \\ \mathbf{0} \\ \mathbf{0} \\ \mathbf{0} \\ -\mathbf{q}_w^{\text{tot}} \end{bmatrix}. \quad (7)$$

Here  $\mathbf{B}_w$  is a block-diagonal matrix with  $N_w$  blocks, for which block  $\mathbf{B}_k$  is a  $n_k \times n_k$  diagonal matrix with entries  $\{\mathbf{B}_k\}_{ii} = (\lambda(s_{k_i})WI_i^k)^{-1}$ . Likewise,  $\mathbf{D}_w$  is a block-diagonal matrix with  $N_w$  blocks in which block number  $k$  is a  $n_k \times 1$  vector with all entries equal one. The sparse  $n_w \times N$  matrix  $\mathbf{C}_w$  has unit entries in positions  $(i, k_i)$ ,  $i = 1, \dots, n_k$ , and  $\mathbf{V}_w = \mathbf{B}\mathbf{D}_{q_w}\mathbf{C}_w\mathbf{D}_\zeta$ . The vectors  $\mathbf{q}_w$ ,  $\mathbf{p}_w$ , and  $\mathbf{q}_w^{\text{tot}}$  contain the local well rates, well pressures, and total well rates, respectively. Rate-constrained wells are then imposed as Neumann conditions where  $q_{w_k}^{\text{tot}}$  is given, and pressure-constrained wells are imposed as Dirichlet boundary conditions where  $p_{w_k}$  is given. For the latter, we can eliminate the corresponding part of  $\mathbf{p}_w$  to give a slightly reduced linear system.

## The Multiscale Mixed Finite-Element Method

In this section, we extend the MsMFE method (Chen and Hou 2003; Aarnes 2004) to compressible flow described by three-phase, black-oil models. For weakly compressible flows, our new MsMFE method is almost identical to the original MsMFE method for incompressible flow (Aarnes 2004; Aarnes et al. 2008) in the sense that basis functions only account for heterogeneities in the porous medium (and possibly changing mobility), whereas compressibility effects are taken into account when constructing the coarse-scale linear system. Compressibility effects can also be accounted for more directly in the basis functions, but this leads to a more complicated (iterative) method that should only be used when strong compressible effects are encountered.

In the current MsMFE formulation (Aarnes 2004; Aarnes et al. 2008), we consider two grids: a fine grid on which the porosities and permeabilities are given constants in each cell, and a coarsened simulation grid in which each block  $\Omega_i$  consists of a connected set of cells from the underlying fine grid; see Fig. 1. The approximation space for previous versions of the

MsmFE method have consisted of a constant approximation of the pressure on each coarse block, and a set of velocity basis functions associated with each interface between two gridblocks and the boundary face between a well and a block. Below, we will demonstrate how the MsmFE method can be extended to also include subscale fine-grid variation in the basis functions for pressure. Moreover, we present a novel method for deriving the coarse-scale equation as a sum of the fine-scale equations.

**Multiscale Basis Functions.** Consider two neighboring gridblocks  $\Omega_i$  and  $\Omega_j$  and let  $\Omega_{ij}$  be a neighborhood containing  $\Omega_i$  and  $\Omega_j$ . Local basis functions  $\varphi_{ij}$  for pressure and  $\psi_{ij}$  for velocity are constructed by solving

$$\vec{\psi}_{ij} = -\lambda \mathbf{K} \nabla \varphi_{ij}, \quad \nabla \cdot \vec{\psi}_{ij} = \begin{cases} w_i(x), & \text{if } x \in \Omega_i, \\ -w_j(x), & \text{if } x \in \Omega_j, \\ 0, & \text{otherwise,} \end{cases} \quad (8)$$

in  $\Omega_{ij}$  with  $\vec{\psi}_{ij} \cdot \vec{n} = 0$  on  $\partial\Omega_{ij}$ . If  $\Omega_{ij}$  extends beyond  $\Gamma_{ij} = \Omega_i \cup \Omega_j$ , we say that the basis functions are computed using overlap or oversampling. The purpose of the weighting function  $w_i(x)$  is to produce a flow with unit average from  $\Omega_i$  to  $\Omega_j$ ; if  $\Omega_{ij} = \Omega_i \cup \Omega_j$  we get unit average flow over  $\Gamma_{ij}$ . The weighting function is therefore normalized such that its integral over  $\Omega_i$  equals one. We will return to the weight function in the next subsection. To solve Eq. 8 numerically, we will use the mimetic discretization introduced above, that is, we use the elliptic part of Eq. 5 obtained by setting  $\mathbf{P}$ ,  $\mathbf{V}$ , and  $\mathbf{b}_N$  to zero. The corresponding basis function  $\psi_{ij}$  for velocity is represented as a vector of fluxes defined on the set of cell-wise ordered faces in the fine grid. Likewise, the basis function  $\varphi_{ij}$  for pressure is represented as a vector of cell pressures on the fine grid.

Next, we discuss basis functions associated with well-block interfaces. Assume that block  $\Omega_i$  is perforated by well  $w_k$  with boundary  $\gamma_{w_k}$ , let  $\Omega_i^k$  be a neighborhood containing  $\Omega_i$ , and define  $\gamma_i^k = \gamma_{w_k} \cap \partial\Omega_i^k$ . The basis function  $\vec{\psi}_i^k$  is constructed by solving

$$\vec{\psi}_i^k = -\lambda \mathbf{K} \nabla \varphi_i^k, \quad \nabla \cdot \vec{\psi}_i^k = \begin{cases} -w_i(x), & \text{if } x \in \Omega_i, \\ 0, & \text{otherwise,} \end{cases} \quad (9)$$

in  $\Omega_i^k$  with constant  $\varphi_i^k$  on  $\gamma_i^k$  and  $\vec{\psi}_i^k \cdot \vec{n} = 0$  on  $\partial\Omega_i^k \setminus \gamma_i^k$ . The use of overlap is more important for  $\vec{\psi}_i^k$  than for  $\vec{\psi}_{ij}$ . We now let  $\psi_i^k$  and  $\mathbf{q}_i^k$  represent face fluxes and well rates (defined on the total set of fine grid perforations) in the numerical solution of Eq. 9 using the elliptic part of Eq. 7 ( $\mathbf{P}$  and  $\mathbf{V}$  set to zero) with prescribed boundary conditions and source term.

To generate the multiscale hybrid system, we split the block-block basis functions as  $\psi_{ij} = \psi_{ij}^H - \psi_{ij}^H$  such that  $\psi_{ij}^H(E)$  equals  $\psi_{ij}(E)$  if  $E \in \Omega_{ij} \setminus \Omega_j$  and is zero otherwise, and  $\psi_{ij}^H(E)$  is equal to  $-\psi_{ij}(E)$  if  $E \in \Omega_j$  and zero otherwise. Next, we arrange all the *hybrid* basis functions  $\psi_{ij}^H$  as columns in a matrix  $\Psi$ , all  $\psi_i^j$  as columns in a matrix  $\Psi_w$  and all basis well-rates  $\mathbf{q}_i^k$  in matrix  $\mathbf{R}_w$ . Similarly, we can organize the corresponding fine-scale pressure basis function in two matrices  $\Phi$  and  $\Phi_w$ .

**Coarse-Scale Equations.** The starting point in developing the multiscale system is the assumption that the fine-scale velocity and pressure fields can approximately be expanded in the corresponding spaces spanned by the basis functions (up to coarse-grid constants). For the fluxes and well rates, this means that  $\mathbf{u}^f \approx \Psi \mathbf{u} + \Psi_w \mathbf{q}_w$  and  $\mathbf{q}_w^f \approx \mathbf{R}_w \mathbf{q}_w$ , and for the fine-scale pressure we use

$$\mathbf{p}^f \approx \mathcal{I} \mathbf{p} + \Phi \mathbf{D}_\lambda \mathbf{u} + \Phi_w \mathbf{D}_{\lambda,w} \mathbf{q}_w. \quad (10)$$

Here  $\mathcal{I}$  is the prolongation from blocks to cells (i.e.,  $\mathcal{I}_{ij}$  is one if block number  $j$  contains cell number  $i$  and is zero otherwise). Moreover,  $\mathbf{D}_\lambda$  is a diagonal matrix with entries  $\bar{\lambda}_i^0 / \bar{\lambda}_i$  (i.e., the ratio between the mean mobility used in the computation of the basis functions Eq. 8 and Eq. 9 and the current mean mobility) for each block  $i$ . The pressure basis functions are unique only up to an additive constant and we may thus choose representations that are orthogonal to the corresponding weighting functions. Specifically, we choose the additive constants such that the functions  $\varphi_{ij}$  satisfy  $\int_{\Omega_i} \varphi_{ij} w_i = 0$  for all  $i, j$ . Consequently, the block-pressures  $\mathbf{p}$  on the coarse grid may be interpreted as a *w-weighted average* of the cell-pressures  $\mathbf{p}^f$  from the fine grid. To simplify the coarse-scale equations, we choose the face-pressures  $\boldsymbol{\pi}$  of the coarse grid to be  $\pi_i = \int_{\Gamma_{ij}} \pi^f \vec{\psi}_{ij} \cdot \vec{n}$ . Finally, we define the prolongation  $\mathcal{J}$  from coarse to fine faces such that  $\mathcal{J}_{ij}$  equals one if coarse face number  $j$  contains fine face number  $i$  and is zero otherwise.

The multiscale system is now obtained by summing the fine-grid equations Eq. 7 as follows ( $\mathbf{I}$  is the identity matrix):

$$\begin{bmatrix} \Psi^T & \mathbf{0} & \mathbf{0} & \mathbf{0} & \mathbf{0} \\ \Psi_w^T & \mathbf{R}_w^T & \mathbf{0} & \mathbf{0} & \mathbf{0} \\ \mathbf{0} & \mathbf{0} & \mathcal{I}^T & \mathbf{0} & \mathbf{0} \\ \mathbf{0} & \mathbf{0} & \mathbf{0} & \mathcal{J}^T & \mathbf{0} \\ \mathbf{0} & \mathbf{0} & \mathbf{0} & \mathbf{0} & \mathbf{I} \end{bmatrix} \begin{bmatrix} \mathbf{B} & \mathbf{0} & \mathbf{C} & \mathbf{D} & \mathbf{0} \\ \mathbf{0} & \mathbf{B}_w & \mathbf{C}_w & \mathbf{0} & \mathbf{D}_w \\ \tilde{\mathbf{C}}^T & \tilde{\mathbf{C}}_w^T & \mathbf{P} & \mathbf{0} & \mathbf{0} \\ \mathbf{D}^T & \mathbf{0} & \mathbf{0} & \mathbf{0} & \mathbf{0} \\ \mathbf{0} & \mathbf{D}_w^T & \mathbf{0} & \mathbf{0} & \mathbf{0} \end{bmatrix}^f \begin{bmatrix} \mathbf{u}^f \\ -\mathbf{q}_w^f \\ -\mathbf{p}^f \\ \boldsymbol{\pi}^f \\ \mathbf{p}_w^f \end{bmatrix} = \begin{bmatrix} \mathbf{0} \\ \mathbf{0} \\ \mathcal{I}^T \mathbf{P}^f \mathbf{p}^{n,f} \\ \mathbf{0} \\ -\mathbf{q}_w^{\text{tot}} \end{bmatrix}. \quad (11)$$

With the above choices of coarse gridblock-pressure and face-pressure, the coarse grid system becomes

$$\begin{bmatrix} B_{11} & B_{12} & C & D & 0 \\ B_{12}^\top & B_{22} & C_w & 0 & D_w \\ \tilde{C}^\top & \tilde{C}_w^\top & P & 0 & 0 \\ D^\top & 0 & 0 & 0 & 0 \\ 0 & D_w^\top & 0 & 0 & 0 \end{bmatrix} \begin{bmatrix} \mathbf{u} \\ -\mathbf{q}_w \\ -p \\ \pi \\ p_w \end{bmatrix} = \begin{bmatrix} 0 \\ 0 \\ \mathcal{I}^\top \mathbf{P}^f \mathbf{p}^{n,f} \\ 0 \\ -q_w^{\text{tot}} \end{bmatrix}. \quad (12)$$

where

$$\begin{aligned} B_{11} &= \Psi^\top B^f \Psi, & B_{12} &= \Psi^\top B_w^f \Psi_w, & B_{22} &= \Psi_w^\top B^f \Psi_w + R_w^\top B_w^f R_w. \\ C &= \Psi^\top C^f \mathcal{I}, & C_w &= (\Psi_w^\top C^f + R_w^\top C_w^f) \mathcal{I}, \\ D &= \Psi^\top D^f \mathcal{J}, & D_w &= R_w^\top D_w^f, & P &= \mathcal{I}^\top P^f \mathcal{I}, \\ \tilde{C} &= C - \Psi^\top V^f \mathcal{I} - D_\lambda \Phi^\top P^f \mathcal{I}, & \tilde{C}_w &= C_w - (\Psi_w^\top V^f + R_w^\top V_w^f) \mathcal{I} + D_{\lambda,w} \Phi_w^\top P^f \mathcal{I}. \end{aligned}$$

If the basis functions are computed without overlap, the  $B$ -part of Eq. 12 is block-diagonal with respect to the coarse gridblocks  $\Omega_i$ , and thus Eq. 12 can be reduced to a symmetric positive-definite system for  $\pi$  and the unknown entries of  $\mathbf{p}_w$ . When overlap is used, one is in general better off using a mixed formulation of Eq. 12. Once the nonlinear iteration in Eq. 12 has converged, fluxes and well-rates can be obtained on the fine grid by  $\mathbf{u}^f = \Psi \mathbf{u} + \Psi_w \mathbf{q}_w$  and  $\mathbf{q}_w^f = R_w \mathbf{q}_w$ , respectively.

**The Weighting Functions.** In previous work, the weighting function has been chosen on the form  $w_i(\theta) = \theta(x)/(\int_{\Omega_i} \theta(x) dx)$ , with varying choices of  $\theta$ : Chen and Hou (2003) used  $\theta = 1$ ; Aarnes (2004) used  $\theta = q$  if  $\int_{\Omega_i} q \neq 0$  and  $\theta = 1$  elsewhere; and Aarnes et al. (2006, 2008) used  $\theta = q$  if  $\int_{\Omega_i} q \neq 0$  and  $\theta = \text{trace}(\lambda \mathbf{K})$ . To understand how these definitions have come into play, and more generally the role that  $\theta$  plays in the multiscale formulation, recall first that the velocity solution is a linear combination of the velocity basis functions. Hence,

$$\nabla \cdot \vec{u}|_{\Omega_i} = \sum_j u_{ij} \nabla \cdot \psi_{ij} = w_i(\theta) \sum_j u_{ij} = w_i(\theta) \oint_{\partial\Omega_i} \vec{u} \cdot \vec{n} ds = w_i(\theta) \int_{\Omega_i} \nabla \cdot \vec{u} dx. \quad (13)$$

Thus, the role of the weighting function  $w_i(\theta)$  is to distribute  $\text{div}(\vec{u})$  onto the fine grid in an appropriate way.

For incompressible flow problems,  $\text{div}(\vec{u})$  is nonzero only in gridblocks with a source, i.e., where  $\int_{\Omega_i} q \neq 0$ . Then, the choice  $\theta = q$  was motivated by the fact that it ensures that the MsMFE method produces mass-conservative velocity fields on the subgrid scale. In gridblocks where the velocity is divergence free,  $\theta$  can be chosen more arbitrarily. The idea of letting the weight function scale with the trace of the mobility was introduced by Aarnes et al. (2006) as a way of avoiding unnaturally strong flow through flow barriers; however, in the absence of regions with (very) low permeability, using  $\theta = 1$  gives (almost) equally accurate results.

For compressible flow problems, we may no longer choose the weight functions arbitrarily. For instance, defining base functions using  $\theta = q$  would concentrate all compressibility effects where  $q$  is non-zero. To avoid this one has to separate the contribution to the divergence field stemming from sources and compressibility. Herein, we impose wells as boundary conditions and may therefore regard  $\Omega$  as source-free. Hence, Eq. 2 may be rewritten as

$$\nabla \cdot \vec{u} = \zeta \vec{u} \cdot (\lambda \mathbf{K})^{-1} \vec{u} - c_t \frac{\partial p}{\partial t}. \quad (14)$$

Ideally,  $\theta$  should therefore be proportional to the right-hand side of Eq. 14. In general, this requires updating  $\theta$  and recomputing the multiscale basis functions frequently, which is undesirable because it significantly impacts the computational cost. Moreover, it is generally difficult to evaluate the right-hand side of Eq. 14 accurately. We will therefore instead make some simplifying approximations. As a motivation, we remark that in most cases, the multiscale concept is not to reproduce the solution of the fine-scale equation, but to account for subgrid effects that strongly influence flow on the coarse grid. To this end, it may be sufficient to account for compressibility on the coarse scale. We therefore propose to use  $\theta = \phi$  whenever the accumulation term is dominating. To motivate this choice, note that since  $p$  is piecewise constant on the coarse grid, the term  $c_t \frac{\partial p}{\partial t}$  is locally proportional to  $c_t$ , and, in turn, to  $\phi$  when the saturations are smooth. Using  $\theta = \phi$  is in accordance with the idea behind using  $\theta = \text{trace}(\lambda \mathbf{K})$ . Indeed, regions with very low permeability tend to also have low porosity, so by choosing  $\theta = \phi$ , one should (to some extent) avoid forcing too much flow through low permeable barriers (Aarnes et al. 2006). Using  $\theta = \text{trace}(\lambda \mathbf{K})$ , on the other hand, will generally give velocity solutions for which  $\text{div}(\vec{u})$  is underestimated in low-permeable regions and overestimated in high-permeable regions.

Even if we choose  $\theta = \phi$ , the basis functions remain time-dependent through the total mobility in Eq. 8 and Eq. 9, which depends on the saturation. This dependence can be handled by using an adaptive criterion as suggested by Jenny et al. (2004) posed in terms of the total mobility  $\lambda$ , or alternatively by replacing  $\lambda \mathbf{K}$  by  $\mathbf{K}$ , thereby rendering the basis functions time-independent.

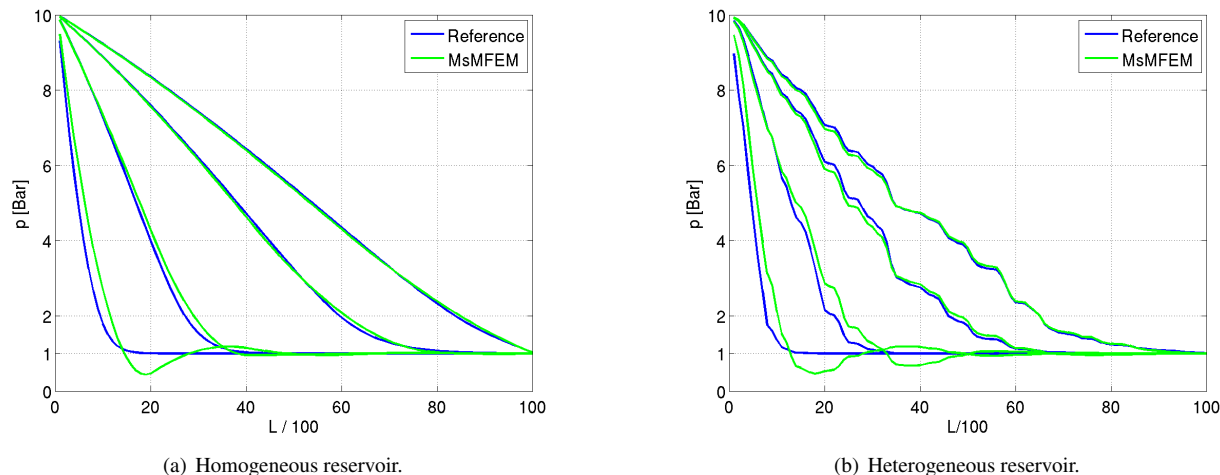


**Fig. 2—Test of effects of compressibility in the MsMFE method. Pressure signal in test example taken from Lunati and Jenny (2006). The multiscale method shows satisfactory agreement with the reference solution after an initial period of pressure oscillations.**

## Numerical Experiments

In this section we explore the performance of the MsMFE method through a series of test cases designed to highlight particular features of the numerical solution. The first example exaggerates effects of fluid compressibility and permeability contrasts while the remaining tests show that the method used in discretizing the local problem greatly affects the accuracy of the overall numerical solution. Moreover, when the flux and pressure basis functions are correctly generated, the MsMFE method captures important characteristics of the flow pattern—even across faults with non-matching gridblock interfaces.

**Tracer Transport in Gas.** This example is taken from Lunati and Jenny (2006) (for more results, see Zhou and Tchalepi 2008). We consider a one-dimensional homogeneous reservoir that is initially at atmospheric pressure ( $p = 0.1$  MPa) and saturated with air. At the left boundary we inject an ideal tracer at a constant pressure of  $p = 1$  MPa, while the pressure at the right boundary is kept fixed at  $p = 0.1$  MPa. Because of the relatively low pressures involved, at least compared with realistic reservoir pressures, this test greatly emphasizes the effects of compressibility and consequently presents a challenging case for our numerical method.

We partition the reservoir into a grid consisting of 100 cells of equal size and superimpose a coarse grid with five equally-sized, coarse gridblocks. **Fig. 2a** shows the resulting pressure signal after 1, 10, 50, and 100 pressure steps. The time increment in each pressure step is  $\tau/400$ , where  $\tau = \mu\phi L^2/(k\Delta p)$  is an estimate of the time required to reach steady state. The reference solution (blue line) is obtained from a mimetic finite-difference discretization of the form Eq. 7, while the MsMFE solution (green line) is computed using Eq. 12. Although the pressure signal is not monotonous in the early stages of the process, the multiscale solution is quickly adjusted to provide agreement with the reference solution. We specifically remark that by using Eq. 10 with pressure basis functions  $\Phi$  and  $\Phi_w$  gives a pressure signal that is fully resolved on the fine scale. This is in contrast to earlier versions of the MsMFE method, which only have had a constant pressure approximation within each coarse gridblock. Moreover, we emphasize that in the simulations above we did *not* update the basis functions, nor iterate on any time step.

We now repeat the above example with the added complexity of heterogeneous porosity and permeability fields, each ranging across several orders of magnitude. The pressure signal from this test is displayed in Fig. 2b. While the initial pressure oscillations do become more pronounced in this case, there is nevertheless acceptable quality in the overall pressure signal.

**Grid Effects.** In this example we wish to investigate grid effects inherent in the MsMFE method. To this end, we consider a curvilinear grid of  $30 \times 20$  cells as shown in the first plot of **Fig. 3**. The grid represents a homogeneous reservoir with permeability equal to 100 milli-darcy and a porosity of 0.3. The reservoir is initially saturated by a compressible gas at a pressure of 250 bar. At the left boundary, we inject an incompressible water phase at 500 bar, while keeping the right boundary at the initial pressure of 250 bar. No-flow conditions are assumed at the upper and lower boundaries. This type of grid is known to produce severe grid effects for the traditional discretizations like the two-point flux-approximation method (Fig. 3). The mimetic method, which we use as our fine-scale discretization, is designed to reproduce a linear pressure variation exactly and will therefore exhibit no grid effects. We observe that the grid effects are nearly negligible also for the MsMFE method when using a mimetic fine-scale solver to generate pressure basis functions with fine-grid variations. On the other hand, as is evident in the final plot of Fig. 3, if the flux and pressure basis functions are generated with a two-point fine-scale solver, then the MsMFE method remains susceptible to effects of grid distortion (resulting from inaccurate computation of basis functions).

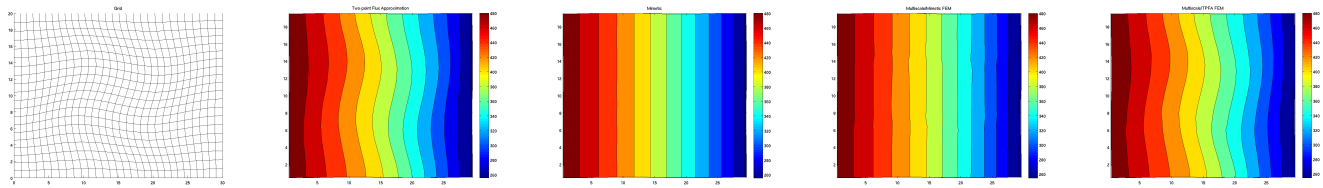
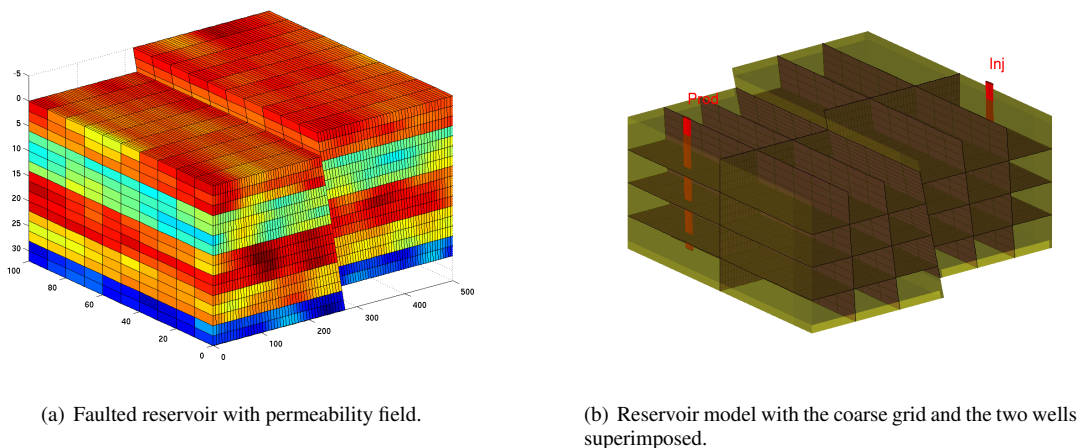


**Fig. 3—Test of grid effects in the MsMFE method. The left plot shows the grid and the next four plots show a comparison of pressure contours for four different methods: the two-point flux-approximation scheme on the fine grid, the mimetic method on the fine grid, the MsMFE method on a  $3 \times 3$  coarse grid with a mimetic discretization of the local problems, and the MsMFE method on the same  $3 \times 3$  coarse grid with a TPFA discretization of the local problems.**



(a) Faulted reservoir with permeability field.

(b) Reservoir model with the coarse grid and the two wells superimposed.

**Fig. 4—Permeability field, well configuration, and coarse grid for the faulted reservoir example.**

**A Reservoir with a Single Fault.** We consider a rectangular reservoir partitioned into  $90 \times 10 \times 16$  gridblocks containing a single fault at which the gridblock interfaces do not match along the fault line. The reservoir and the associated layered permeability field are shown in Fig. 4a. Here, the coarse grid is of dimension  $6 \times 2 \times 4$  blocks, which corresponds to an upscaling factor of 300. Initially, the reservoir is saturated with a compressible oil at 205 bar and we simulate enhanced recovery with a rate-constrained water injector at  $1,000 \text{ m}^3/D$  and a producing well constrained to a bottomhole pressure target of 200 bar. The well configuration and the coarse grid is shown in Fig. 4b. We collect summary results in Fig. 5. The plots show, respectively, well flux in the producing well, water cut in the producing well, pressure in the injector, and relative error in the water saturation compared with the fine-scale reference solution throughout the reservoir as a function of time. We observe that the MsMFE method accurately estimates the well flux and production curves, while there is some discrepancy in the estimates of injector pressure and water saturation in the reservoir. These discrepancies are consistent with previous results observed for the MsMFE method and are to be expected, because we have not employed an iteration strategy (e.g., as proposed by Hajibeygi et al. (2008)) to diminish the reservoir saturation residuals and thereby constructing a complete solution to the problem on the fine scale. However, the MsMFE method still captures important qualitative features of the overall flow pattern and saturation fronts. This aspect of the method is demonstrated in Figs. 6a and 6d, which show snapshots of the reservoir pressure and saturation profiles taken after 250 out of 500 days of simulated production. We specifically remark that the pressure field obtained from the MsMFE method exhibits the same characteristic reservoir pressure drop as the reference solution on the fine scale, even though the absolute pressure drop is greater in the MsMFE solution. Furthermore, the MsMFE saturation profile effectively captures the layered water distribution through the highly permeable regions of the reservoir.

**A Reservoir with Five Faults.** The final example has five curved faults and, consequently, quite complex geometry. The reservoir is initially saturated with a compressible oil at 375 bar and is produced from two wells,  $P1$  and  $P2$ , constrained to bottomhole pressure targets of 250 bar and 300 bar, respectively. We inject incompressible water at a rate of  $1,000 \text{ m}^3/D$  through each of two injection wells,  $I1$  and  $I2$ . This rate corresponds to one pore-volume injected in slightly less than 1,500 days. Fig. 7 shows the permeability field, the well configuration, and the coarse grid. Moreover, Fig. 8 shows a comparison between the reservoir pressure distribution by the MsMFE method (left plot) and by the mimetic reference method (right plot) at the end of the simulation. We observe that the MsMFE method is capable of reproducing a high-quality pressure distribution. Finally, we collect summary results in Fig. 9. The left plot shows the well fluxes in the producing wells,  $P1$  and  $P2$ , and the right

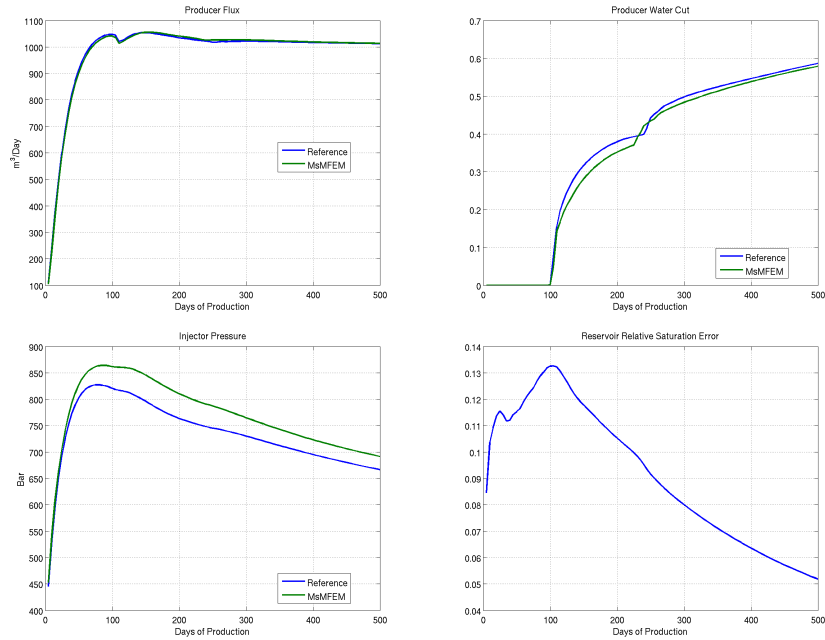


**Fig. 5—Summary results for the faulted reservoir example. The plots show fluxes at the producer, water cuts, pressures at injector, and relative saturation errors, respectively, as function of time.**

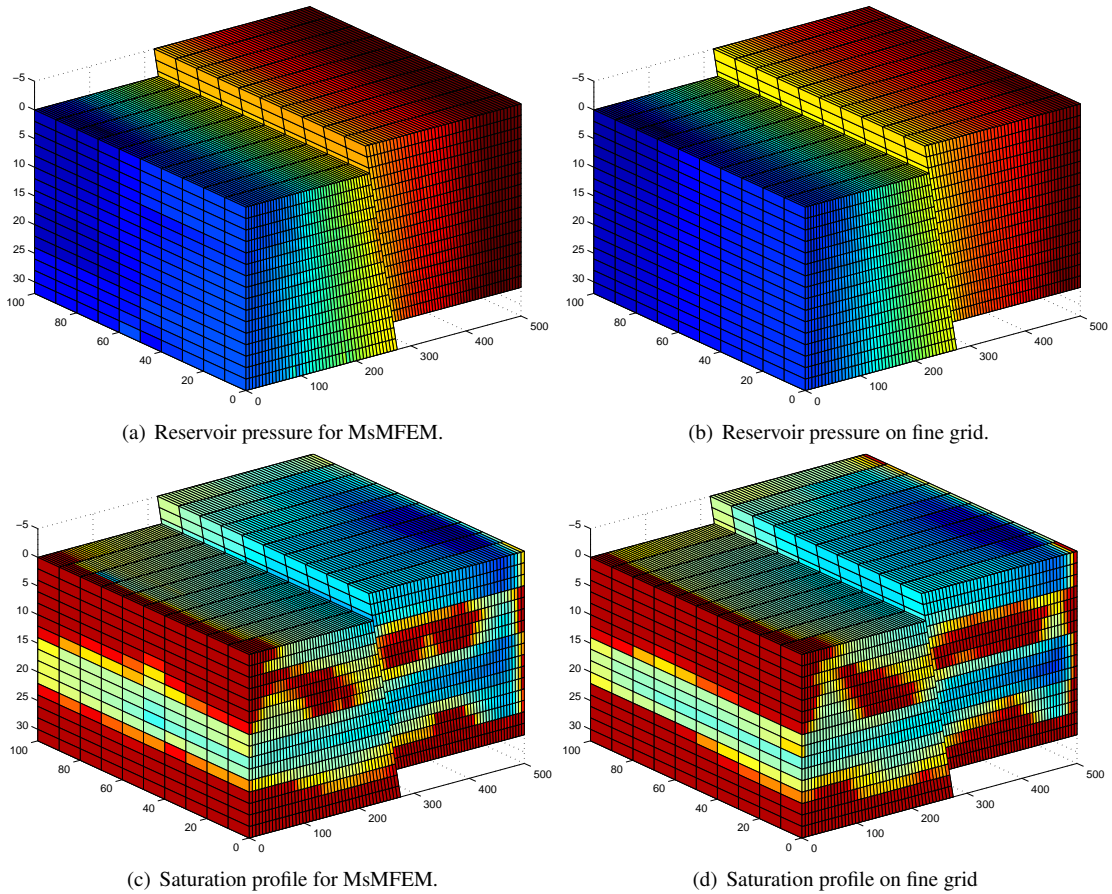


**Fig. 6—Snapshots taken after 250 out of 500 days of production.**

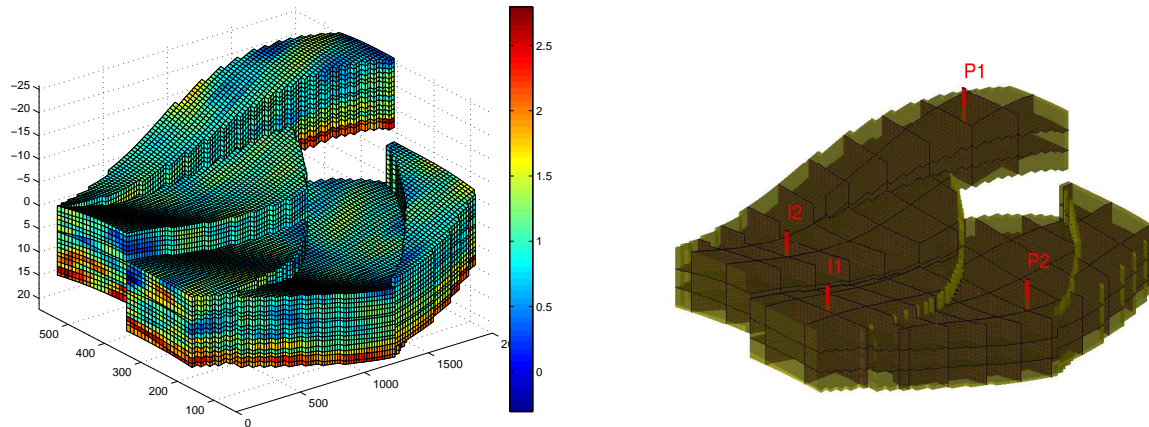


Fig. 7—Permeability field, well configuration, and coarse grid for the reservoir model with five faults.

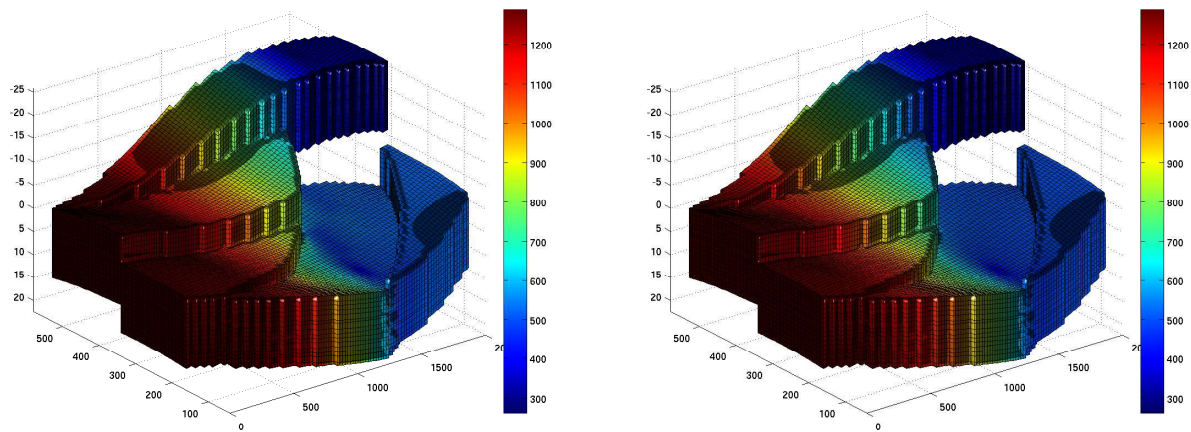


Fig. 8—Comparison of pressure results at end of simulation on realistic reservoir model. The MsMFE method (left) is able to reproduce the fine-scale pressure variation of the reference solution (right).

plot shows water cuts in the producing wells. While these results do show some degradation in the derived quantities compared with the reference solution, particularly for well *P1*, we still submit that the MsMFE method captures essential features of the model. Taking into account that the MsMFE discretization in this case corresponds to an upscaling factor of roughly 305, the results are quite encouraging.

## Conclusions

We have presented a first attempt to extend the MsMFE method to compressible black-oil models and have developed a formulation that gives subscale resolution in both pressure and velocity. The development is strongly motivated by streamline simulation, in which a sequential splitting is used to decouple flow and transport. Herein, however, we have used a simple explicit single-point upwind method to solve the hyperbolic transport equations. Through several numerical examples, we demonstrated that the resulting simulator is able to incorporate moderate compressibility effects while retaining the ability to resolve fine-scale flow details and complex grid geometry. The results show that the MsMFE method can be used to bypass upscaling and enable direct simulation of high-resolution geological models. Indeed, Natvig et al. (2009) recently demonstrated use of the MsMFE pressure solver within a streamline simulator to give a robust, efficient, and very flexible method for simulating highly resolved models of complex fractured reservoirs in which fractures and fracture corridors are represented as explicit volumetric objects.

The current version of the MsMFE method can mainly be characterized as an efficient and approximate pressure solver that is capable of including subscale flow details. If the method is to achieve full accuracy on the fine scale, further research is needed to develop a more robust splitting method that involves adaptive updating of basis functions, nonlinear pressure iterations, and more accurate schemes for reconstructing flow fields, e.g., along the lines of (Hajibeygi et al. 2008).

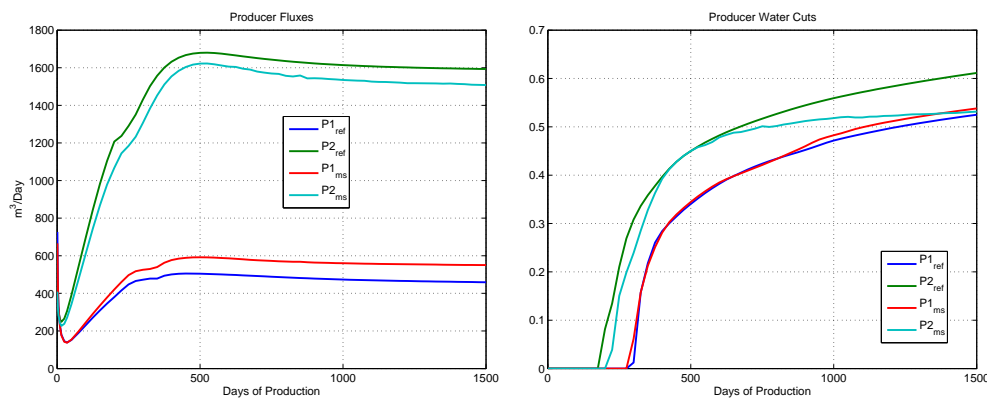


Fig. 9—Producing well fluxes and water cuts as a function of time.

## Acknowledgments

The authors gratefully acknowledge financial support from the Research Council of Norway under grants number 174551/S30, 178013/I30, and 186935/I30.

## Nomenclature

### Physical quantities:

$b_\ell$	=	volume factor for phase $\ell$
$c_\ell$	=	phase compressibility
$c_t$	=	total compressibility
$f$	=	fractional flow
$k_r$	=	relative permeability
$\mathbf{K}$	=	absolute permeability
$p$	=	pressure
$s$	=	saturation
$t$	=	time
$\vec{u}$	=	total Darcy velocity
$x$	=	spatial coordinate
$q$	=	volumetric rate
$q_w^{\text{tot}}$	=	total rate of well $w$
$q_i^k$	=	rate of well $k$ in cell/block $i$
$WI$	=	well index
$WI_i^k$	=	well index of well $k$ in cell $i$
$\lambda$	=	total mobility
$\mu$	=	viscosity
$\phi$	=	porosity
$\pi$	=	face pressure

### Vectors and matrices:

$\mathbf{s}$	=	vector of cell/block saturations
$\mathbf{p}$	=	vector of cell/block pressures
$\boldsymbol{\pi}$	=	vector of cell/block face pressures
$\mathbf{u}$	=	vector of outward fluxes on cell/block faces
$\mathbf{B}$	=	inner product of velocity basis functions
$\mathbf{C}$	=	integral of the divergence of velocity b.f.
$\mathbf{D}$	=	map from local to global face numbering
$\mathbf{P}$	=	compressibility matrix
$\mathbf{T}_E$	=	transmissibility matrix for cell $E$
$\mathbf{V}$	=	integral of quadratic velocity terms
$\boldsymbol{\Psi}$	=	matrix of all basis functions
$\mathbf{R}_w$	=	matrix of well rates $q_i^k$

### Domain and grid:

$\Omega$	=	entire physical domain
$\partial D$	=	boundary of domain $D$
$E$	=	cell in the fine grid
$\Omega_i$	=	coarse block number $i$
$\Omega_{ij}$	=	support for basis function $\vec{\psi}_{ij}$
$\Omega_i^k$	=	support for basis function $\vec{\psi}_i^k$
$\gamma_w$	=	boundary of well $w$
$\gamma_i^k$	=	interface between well $w$ and $\Omega_i^k$

### Basis functions, etc:

$\vec{\psi}_{ij}$	=	basis function, interface of block $i$ and $j$
$\vec{\psi}_i^k$	=	basis function, interface of block $i$ and well $k$
$w_i$	=	weight function associated with coarse block $\Omega_i$
$\theta$	=	distribution function used in the weight function $w_i$

### Numbers:

$N$	=	number of cells in fine grid
$N_w$	=	number of wells
$n_E$	=	number of faces in cell $E$
$n_k$	=	number of cells perforated by well $k$

### Subscripts:

$i, j, k_i$	=	block/cell numbers
$k$	=	well number
$\ell$	=	Phase number (o=oil, w=water, g=gas)
$\nu$	=	iteration number
$w$	=	well number

### Superscripts:

$k$	=	well number
$n$	=	time step

## References

- Aarnes, J. E. 2004. On the Use of a Mixed Multiscale Finite Element Method for Greater Flexibility and Increased Speed or Improved Accuracy in Reservoir Simulation. *Multiscale Model. Simul.*, 2(3):421–439 (electronic).
- Aarnes, J. E., Krogstad, S., and Lie, K.-A. 2006. A Hierarchical Multiscale Method for Two-Phase Flow Based Upon Mixed Finite Elements and Nonuniform Coarse Grids. *Multiscale Model. Simul.*, 5(2):337–363 (electronic).
- Aarnes, J. E., Krogstad, S., and Lie, K.-A. 2008. Multiscale Mixed/Mimetic Methods on Corner-Point Grids. *Comput. Geosci.*, 12(3):297–315. Doi:10.1007/s10596-007-9072-8.
- Aziz, K. and Settari, A. 1979. *Petroleum Reservoir Simulation*. Elsevier Applied Science Publishers, London and New York.
- Brezzi, F. and Fortin, M. 1991. *Mixed and Hybrid Finite Element Methods*, volume 15 of *Springer Series in Computational Mathematics*. Springer-Verlag, New York.
- Brezzi, F., Lipnikov, K., and Simoncini, V. 2005. A Family of Mimetic Finite Difference Methods on Polygonal and Polyhedral Meshes. *Math. Models Methods Appl. Sci.*, 15:1533–1553.
- Chen, Z. and Hou, T. 2003. A Mixed Multiscale Finite Element Method for Elliptic Problems With Oscillating Coefficients. *Math. Comp.*, 72:541–576.
- Hajibeygi, H., Bonfigli, G., Hesse, M. A., and Jenny, P. 2008. Iterative Multiscale Finite-Volume Method. *J. Comput. Phys.*, 227(19):8604–8621.
- Hou, T. and Wu, X.-H. 1997. A Multiscale Finite Element Method for Elliptic Problems in Composite Materials and Porous Media. *J. Comput. Phys.*, 134:169–189.
- Jenny, P., Lee, S. H., and Tchelepi, H. A. 2004. Adaptive Multiscale Finite-Volume Method for Multiphase Flow and Transport in Porous Media. *Multiscale Model. Simul.*, 3(1):50–64 (electronic).
- Jenny, P., Lee, S. H., and Tchelepi, H. A. 2003. Multi-Scale Finite-Volume Method for Elliptic Problems in Subsurface Flow Simulation. *J. Comput. Phys.*, 187:47–67.
- Jenny, P., Lee, S. H., and Tchelepi, H. A. 2006. Adaptive Fully Implicit Multi-Scale Finite-Volume Method for Multi-Phase Flow and Transport in Heterogeneous Porous Media. *J. Comput. Phys.*, 217(2):627–641.
- Juanes, R. and Tchelepi, H. A. 2008. Special Issue on Multiscale Methods for Flow and Transport In Heterogeneous Porous Media. *Comput. Geosci.*, 12(3):255–416.
- Kippe, V., Aarnes, J., and Lie, K.-A. 2008. A Comparison of Multiscale Methods for Elliptic Problems in Porous Media Flow. *Comput. Geosci.*, 12(3):377–398. Doi: 10.1007/s10596-007-9074-6.
- Lee, S. H., Wolfsteiner, C., and Tchelepi, H. 2008. Multiscale Finite-Volume Formulation for Multiphase Flow in Porous Media: Black Oil Formulation of Compressible, Three Phase Flow With Gravity. *Comput. Geosci.*, 12(3):351–366. Doi:10.1007/s10596-007-9069-3.
- Lu, B., Alshaaan, T. M., and Wheeler, M. F. 2007. Iteratively Coupled Reservoir Simulation for Multiphase Flow. Paper SPE 110114 presented at SPE Annual Technical Conference and Exhibition, Anaheim, California, U.S.A., 11–14 November.
- Lunati, I. and Jenny, P. 2006. Multiscale Finite-Volume Method for Compressible Multiphase Flow in Porous Media. *J. Comput. Phys.*, 216(2):616–636.
- Lunati, I. and Jenny, P. 2008. Multiscale Finite-Volume Method for Density-Driven Flow in Porous Media. *Comput. Geosci.*, 12(3):337–350.
- Natvig, J. R., Skaflestad, B., Bratvedt, F., Bratvedt, K., Lie, K.-A., Laptev, V., and Khataniar, S. K. 2009. Multiscale Mimetic Solvers for Efficient Streamline Simulation of Fractured Reservoirs. Paper SPE 119132 presented at 2009 SPE Reservoir Simulation Symposium, The Woodlands, Texas, USA, 2–4 February.
- Peaceman, D. 1983. Interpretation of Well-Block Pressures in Numerical Reservoir Simulation With Nonsquare Grid Blocks and Anisotropic Permeability. *SPE J.*, 23(3):531–543. SPE 10528-PA. Doi:10.2118/10528-PA.
- Skaflestad, B. and Krogstad, S. 2008. Multiscale/Mimetic Pressure Solvers With Near-Well Grid Adaption. In *Proceedings of ECMOR XI—11th European Conference on the Mathematics of Oil Recovery*, number A36, Bergen, Norway. EAGE.
- Tchelepi, H., Jenny, P., Lee, S., and Wolfsteiner, C. 2007. Adaptive Multiscale Finite Volume Framework for Reservoir Simulation. *SPE J.*, 12:188–195. Doi: 10.2118/93395-PA.
- Zhou, H. and Tchelepi, H. 2008. Operator-Based Multiscale Method for Compressible Flow. *SPE J.*, 13(2):267–273.